applied sciences

MDPI

Article

FTIR and Raman Characterization of TiO_2 Nanoparticles Coated with Polyethylene Glycol as Carrier for 2-Methoxyestradiol

Andrea León [1,2,*], Patricia Reuquen [2,3], Carolina Garín [1], Rodrigo Segura [4], Patricio Vargas [1,2], Paula Zapata [5] and Pedro A. Orihuela [2,3]

1 Departamento de Física, Universidad Técnica Federico Santa María, Valparaíso 2340000, Chile; carolina.garin@usm.cl (C.G.); patricio.vargas@usm.cl (P.V.)
2 Centro del Desarrollo para la Nanociencia y Nanotecnología-CEDENNA, Universidad de Santiago de Chile, Santiago 8320000, Chile; patricia.reuquen@usach.cl (P.R.); pedro.orihuela@usach.cl (P.A.O.)
3 Laboratorio de Inmunología de la Reproducción, Facultad de Química y Biología, Universidad de Santiago de Chile, Santiago 8320000, Chile
4 Instituto de Quimica y Bioquímica, Facultad de Ciencias, Universidad de Valparaíso, Valparaíso 2340000, Chile; rodrigo.segura@uv.cl
5 Grupo Polímeros, Facultad de Química y Biología, Universidad de Santiago de Chile, Santiago 8320000, Chile; paula.zapata@usach.cl
* Correspondence: andrea.leon@postgrado.usm.cl; Tel.: +56-322654555

Academic Editor: Jordi Puiggalí
Received: 16 September 2016; Accepted: 11 November 2016; Published: 4 January 2017

Abstract: The aim of this study was to prepare a novel targeting drug delivery system for 2-Methoxyestradiol (2ME) in order to improve the clinical application of this antitumor drug. It is based in nanoparticles (NPs) of titanium dioxide (TiO_2) coated with polyethylene glycol (PEG) and loaded with 2ME. A complete IR and Raman characterization have been made to confirm the formation of TiO_2–PEG–2ME composite. Vibrational modes have been assigned for TiO_2, PEG, and 2ME and functionalized TiO_2–PEG and TiO_2–PEG–2ME. The observed variation in peak position of FTIR and Raman of each for these composites has been elucidated in terms of intermolecular interactions between PEG–2ME and TiO_2, obtaining step-by-step the modification processes that were attributed to the conjugation of PEG and 2ME to TiO_2 NPs. Modifying TiO_2 NPs with PEG loaded with the 2ME drug revealed that the titanium dioxide nanocarrier possesses an effective adsorption capability, and we discuss their potential application as a system of drug delivery.

Keywords: TiO_2 NPs; drug delivery; 2-Methoxyestradiol; anticancer drug; TiO_2-2ME NPs

1. Introduction

Due to the unique properties afforded by their size, nanoparticles (NPs) possess a wide range of applications in the industrial, electrical, agricultural, pharmaceutical, and medical fields. For anticancer applications, nanoparticles can be easily modified and conjugated with multiple functionalities, such as targeting molecules, imaging agents, and drugs [1,2]. Nanoparticles are used as a drug carrier for the specific delivery of drugs to cancer cells. In targeted drug delivery, the anticancer drug is delivered specifically to the cancer cells, reducing the toxicity to normal cells.

Titanium dioxide (TiO_2) is considered to be a potential semiconductor for biocidal applications due to its photocatalytic properties, which explain its ability to destroy bacteria, viruses, and even cancer cells [3,4]. In this context, TiO_2 NPs have considerable potential in biomedicines, and a variety of works have been conducted to develop new antibacterial and drug delivery systems based on this nanoparticle [5–8]. Additionally, TiO_2 has been classified as a biologically inert substance in animals and humans [9,10], and it has good biocompatibility and no toxicity in vitro or in vivo [11].

The application of TiO_2 NPs in biosystems may be difficult, due to their poor dispersibility and stability in water or biological sera. To improve the colloidal behavior of NPs in biological systems, it is necessary to study the surface properties and colloidal stability of TiO_2 NPs [11–13]. Recent studies have focused on covering the surface of TiO_2 NPs with polymeric materials to eliminate aggregation and sedimentation [11,14], reduce toxicity, and develop biocompatibility [15]. In this context, polyethylene glycol (PEG)—due to its hydrophilic character—permits the modification of the surface of NPs in order to prevent agglomeration, and also renders NPs resistant to protein adsorption and enhances their biocompatibility [15–17].

2-Methoxyestradiol (2ME) is an endogenous estrogen metabolite with antiangiogenic and anticancer properties, although it has a poor solubility and low bioavailability for in vivo models [18]. With the purpose of maintaining its high anticancer efficacy, different reports are found in the literature about the incorporation of 2ME in different types of NPs, such as metallic NPs [19,20], polymerics NPs, and other nanostructured materials [21,22]. These studies confirm that NPs conjugated with 2ME are more effective from the point of view of cancer cell killing in comparison to 2ME alone. In this work, based on the suitable properties of TiO_2 and PEG, as well as the potential use of 2ME in the treatment of many cancer types [18], we formulated 2ME-loaded TiO_2–PEG nanoparticles that protect the anticancer agent from early degradation. TiO_2 nanoparticles were modified with PEG to improve their suspension stability, and then 2ME was loaded on TiO_2–PEG conjugate (TiO_2–PEG–2ME). This research was performed based on the possibility of the combined application of TiO_2 NPs (as a nanocarrier) with PEG (to improve the colloidal stability) and 2ME (as an anticancer drug).

2. Materials and Methods

2.1. Synthesis of TiO_2 Nanoparticles

TiO_2 nanospheres were synthesized using the sol–gel method [23]. The reagents used in the synthesis of the nanoparticles and in their organic modifications were titanium isopropoxide (TTIP; Aldrich, reagent grade, 99%), isopropanol, nitric acid (HNO_3), distilled water, and hexadecyl trimethoxysilane (Mod-TiO_2) (Aldrich, reagent grade, 98%) was used for the modification of TiO_2 nanoparticles [24].

2.2. Modification of TiO_2 NPs by PEG

TiO_2 NPs need to be modified to prevent their aggregation and sedimentation. One of the most well known methods for the modification of NPs is covering them with polymeric materials [15,17]. In this study, PEG 6000 (Sigma Aldrich, St. Louis, MO, USA) was used as the modification agent. In order to conjugate PEG to TiO_2 NPs, 100 mL of the suspension with a TiO_2 concentration of 1 g/L was prepared. After sonication for 2 h, 200 mg PEG was added, and the reaction mixture was sonicated for 3 h. The PEG–TiO_2 NPs were centrifuged at 5000 rpm for 30 min at 25 °C. After modification, the PEG–TiO_2 NPs were dried at 60 °C for 1 h.

2.3. Drug Encapsulation and Loading Efficiencies

TiO_2–PEG NPs (0.1 mg) were dispersed in 10 mL distilled water, and then 100 µL of 2ME (Sigma Aldrich) at a concentration 10 µg/µL was added and stirred smoothly for 3 h. After modification, the TiO_2–PEG–2ME NPs were dried at 60 °C for 1 h. For each sample, 100 µL of TiO_2–PEG–2ME was filtered using 0.45 µm polyvinylidene difluoride (PVDF) membrane syringe filters (Merck, Kenilworth, NJ, USA), and the flow-trough was centrifuged at 10,000 rpm per min at 4 °C. Samples (20 µL) were injected into the Reodyne valve of a liquid chromatograph (Agilent 1200s, Palo Alto, CA, USA), and were separated in a reverse phase column C18 (150 × 4.6 mm, 5 µm; Agilent, Zorbax, XDB-C18) at room temperature with formic acid 0.1%:methanol (8:92) with flow of 0.5 mL/min for 30 min. The detection was performed using an electrospray ionization triple quad tandem mass spectrometer (Agilent 6410, Palo Alto, CA, USA) in negative mode, with 300 °C temperature, 3500 V

ionization voltage, and 8 L/min of nitrogen flow. Quantitation was performed using the multiple reaction monitoring (MRM) mode, with experimental determination of majoritarian mass-charge ratios (m/z) (2-MeOE2: 301 → 286). The working curve was obtained by standard 2ME solutions with different concentrations. The loading amounts (L_A) were calculated using the equation

$$L_A(wt\%) = \frac{2ME_T - 2ME_{ST}}{2ME_T}, \quad (1)$$

where $2ME_T$ is 2ME total and $2ME_{ST}$ is 2ME in the supernatant.

A schematic representation of TiO_2–PEG conjugation and 2-ME drug loading in the TiO_2–PEG composite is shown in Figure 1.

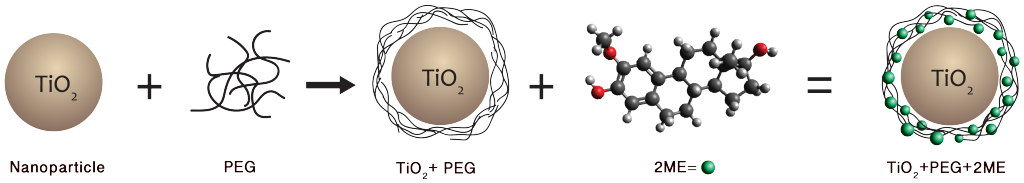

Figure 1. Schematic representation of the functionalization of PEG–TiO_2 and TiO_2–PEG–2ME (2ME image is supported by [25]). (2ME: 2-Methoxyestradiol; PEG: polyethylene glycol.)

2.4. Characterization of TiO_2, TiO_2–PEG, and TiO_2–PEG–2ME NPs

The morphology of TiO_2 NPs was analyzed by transmission electron microscopy (TEM) using a JEOL ARM 200 F microscope operated with an acceleration voltage of 20 kV. Samples for TEM measurements were prepared by placing a drop of TiO_2 on a carbon-coated standard copper grid (400 mesh) and letting the solvent evaporate.

The functionalization of TiO_2 NPs by PEG and the conjugation of TiO_2–PEG with 2ME were examined by attenuated total reflectance Fourier-transform infrared spectroscopy (ATR-FTIR). The FTIR spectra were collected in the 4000–1000 cm^{-1} range, with a resolution of 4 cm^{-1} at room temperature by using a Thermo Nicolet IS10 spectrometer provided with single bounce Ge crystal Smart-iTR accessory. In order to complement the FTIR spectra, Raman spectroscopy was performed by using a LabRAM HR800 spectrometer provided with a green He-Ne laser (534 nm) as the excitation source. The Raman spectra were collected in the region 3600–100 cm^{-1}, with a spectral resolution of 0.3 cm^{-1}. The number of accumulated scans for each recorded spectrum was two, and the exposure time was 30 s. All of the experiments were performed at room temperature.

3. Results and Discussion

Figure 2 shows transmission electron micrographs of TiO_2 NPs, revealing a quasi-spherical morphology with average diameters of around 10 nm, and a relatively narrow size dispersion characteristic of the sol–gel method.

3.1. FTIR Analysis

Figure 3 shows a sequence of FTIR spectra for TiO_2 NPs, PEG, TiO_2 coated with PEG, 2ME, and composite TiO_2–PEG–2ME. In Figure 3a, the FTIR spectrum of TiO_2 NPs clearly shows tree bands. The first band is the broadest, and is observed at 3500 cm^{-1}, corresponding to the stretching vibration of the hydroxyl group O-H of the TiO_2 NPs. The second band is observed around 1630 cm^{-1}, corresponding to bending modes of water Ti-OH; the last is a prominent peak at 1383 cm^{-1} related to Ti-O modes [26,27]. In Figure 3b, the FTIR spectrum of PEG is shown. The peaks around 2888, 2920, and 2888 cm^{-1} are attributed to the alkyl chain of polymer; the bands at 1342 and 1100 cm^{-1} are due to C-H bending and C-O stretching vibration, respectively; and the band at 1242 cm^{-1} corresponds to C-H twisting vibrations [16,17,26]. The IR spectrum of TiO_2–PEG is given

in Figure 3c, where new bands appear due to the presence of PEG (such as the bands around 2880, 1352, and 1105 cm^{-1}, corresponding to C-H stretching vibrations, C-H bending, and C-O stretching vibration); all these bands are shifted from their original position in PEG, exhibiting hydrogen-bonding nature and confirming PEG's interaction with the surface of TiO_2 NPs.

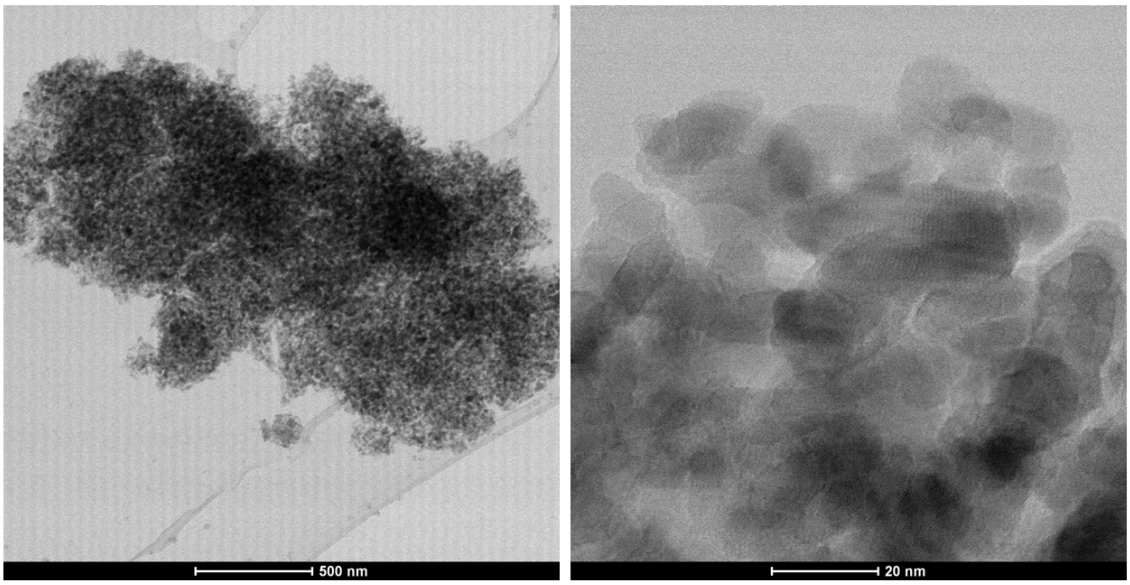

Figure 2. Transmission electron microscopy (TEM) image of TiO_2 nanoparticles (NPs).

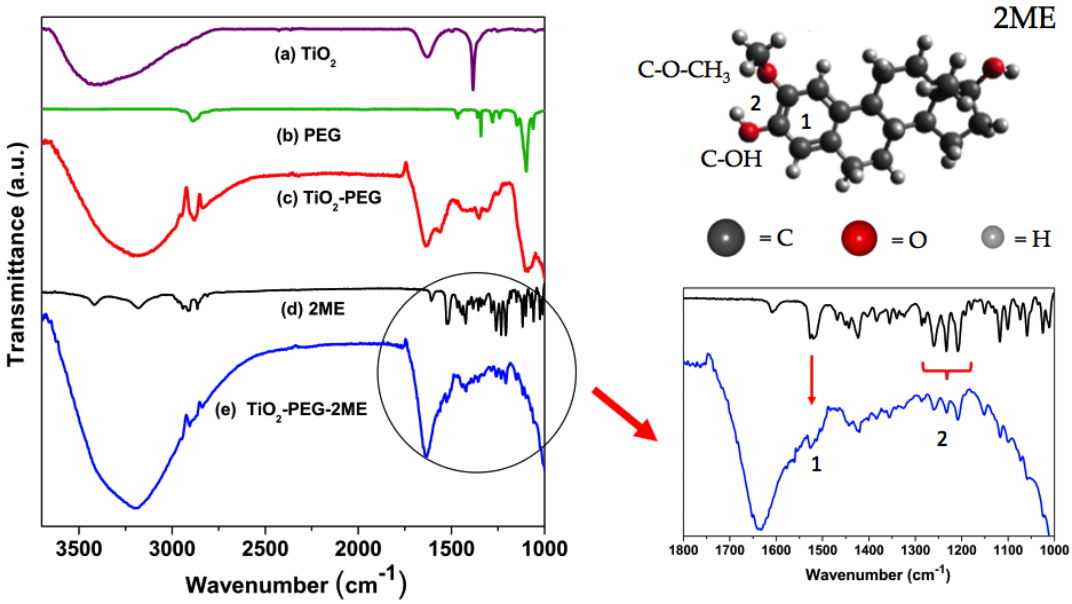

Figure 3. Fourier-transform infrared (FTIR) spectra for (**a**) TiO_2; (**b**) PEG; (**c**) TiO_2–PEG; (**d**) 2ME, and (**e**) TiO_2–PEG–2ME. The magnified view of (**d**) and (**e**) on the right side shows the IR spectrum for TiO_2–PEG–2ME in the range 1800–1000 cm^{-1}; in this zone, it is possible to identify the peaks associated with aromatic ring C=C stretching vibration in of 2ME (zone 1) and tree peak associated with the methoxy group O-CH_3 and the alcohol group C-OH (zone 2); these zones are showed in the upper right side in an schematic representation of the 2-Methoxyestradiol molecule. The color of spheres (gray, red and light gray) represent Carbon (C), Oxigen (O) and Hydrogen (H) atoms.

The FTIR spectrum of 2ME and functionalized TiO_2–PEG NPs with 2ME is given in Figure 3d,e. The FTIR spectrum of 2ME alone is characterized by a number of characteristic bands occurring at 3417, 3182, 3000, 2963, 2907, 2809, and 1600 cm^{-1}, and in the ranges 1500–1400 cm^{-1} and 1300–1000 cm^{-1}; the last bands are the fingerprint of 2ME. The bands between 3417 and 3000 cm^{-1} are due to hydroxyl stretching vibration bands. The band at 3000 cm^{-1} belongs to the C-H bond stretching vibration. The bands at 2963, 2907, and 2809 cm^{-1} correspond to stretching vibration of functional groups CH, CH_2, and CH_3. The vibration at 1600 cm^{-1} corresponds to C=C bond stretching vibration in the aromatic ring (zone 1 in Figure 3). The bands in the range 1500–1400 cm^{-1} are due to CH, CH_2, and CH_3 bending vibration and those in 1300–1200 cm^{-1} correspond to vibration of the methoxy group O-CH_3 and the alcohol group C-OH (zone 2 in Figure 3). In the FTIR spectrum of TiO_2–PEG–2ME in Figure 3e, new bands belonging to 2ME are observed—these bonds occurring mainly in the region 1525–1000 cm^{-1}. In this zone, we can distinguish peaks located at 1525 and 1420 cm^{-1} (zone 2) corresponding to the bending vibration of functional groups CH, CH_2, and CH_3. These bands are shifted from their original position at 1526 and 1422 cm^{-1} in pure 2ME. In zone 1 we found bands appearing at 1260, 1232, and 1205 cm^{-1}, slightly shifted from their original position in 2ME [20,28]. We can identify the most important bands of 2ME corresponding to methoxy and alcohol functional groups. This confirms the attachment of 2ME into the composite TiO_2–PEG.

4. Raman Analysis

In the Figure 4, we can see a complete Raman spectra of TiO_2, PEG, 2-ME, composite TiO_2–PEG, and functionalized TiO_2–PEG–2ME NPs.

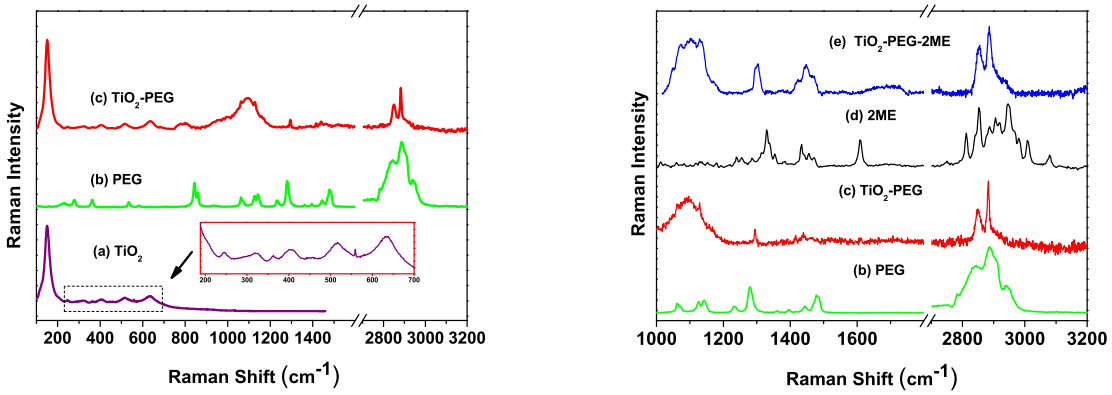

Figure 4. The left and right side graphs show the Raman spectra for (**a**) TiO_2; (**b**) PEG, and (**c**) TiO_2–PEG, recorded in the zone 150–3200 cm^{-1}; (**d**) 2ME; and (**e**) TiO_2–PEG–2ME in the region 1000–3200 cm^{-1}, respectively.

4.1. Raman TiO_2

The anatase phase of TiO_2 NPs has six Raman active modes (A_{1g} + $2B_{1g}$ + $3E_g$). This is shown in Figure 4a, and it is in agreement with other Raman analysis for the anatase phase of TiO_2 NPs [28–30].

4.2. Raman Spectrum PEG

The Raman spectrum of PEG is presented in Figure 4b. The most representative band positions are the stretching vibrations of alkyl chains observed at 2938, 2886, and 2843 cm^{-1} [31–33]; we can see that these vibration groups are more strong in the Raman spectra than in the IR spectra. The bands at 1478 and 1442 cm^{-1} are assigned to the bending mode of the C-H group. The bands that appeared at 1279 and 1229 cm^{-1} correspond to C-H twisting vibrations. The C-O, C-O-H, and C-C stretching vibrations are located in the 1142–1126 cm^{-1} range [32]; this vibrational mode can also be found more

strongly in the IR spectra. The bands at 846 and 860 cm^{-1} are assigned to the skeletal vibrations of PEG [28,34,35]. The positions at 533 and 362 cm^{-1} correspond to C-C-O bending vibration, and the last band at around 225 cm^{-1} corresponds to PEG skeletal deformation mode [33].

4.3. Raman Spectra Analysis of TiO_2–PEG

The Raman active vibrational modes of TiO_2 localized in the range of the 400–600 cm^{-1} band in TiO_2–PEG did not show any appreciable shift, indicating that upon the addition of PEG, the structure of TiO_2 is not affected (Figure 4c). This confirms that the crystalline phase of TiO_2 NPs is preserved in the functionalization process. It should also be mentioned that the intensities in the region between 1000–3200 cm^{-1} have been amplified, because this zone is less intensive compared to the TiO_2 band (the ratio of intensities between the bands of TiO_2 and the bands that arise due to the functionalization with PEG is $\frac{I_{TiO_2}}{I_{TiO_2-PEG}} = 50$).

On the other hand, due to the functionalization of TiO_2's surface with PEG, we can observe a broad peak at around 1000–1200 cm^{-1} attributable to C-C and C-O stretching vibrations. Two sharp peaks between 2800–3000 cm^{-1} are also observed, corresponding to C-H stretching vibration; these peaks confirm the addition of PEG with TiO_2 (Figure 4c). The prominent peak localized in the range of 2800–3000 cm^{-1} corresponds to the stretching vibrations of the methylene group C-H of TiO_2–PEG found at 2883 cm^{-1}; this band is shifted about 3 cm^{-1} from its original position (at 2886 cm^{-1} in pure PEG). This slight shift suggests the formation of hydrogen bridge bonds, these bonds have arisen due to the Van Der Waals interaction between the OH groups of TiO_2 and the hydroxyl group of PEG [28,32,34,35]. These results demonstrate that the surface modification of TiO_2 NPs by PEG is highly influenced by the intermolecular interactions between these two materials. We can observe that the vibration of C-C, C-O, and C-H groups (located in the range 1000–1200 cm^{-1}) are as prominent as in the IR and Raman spectra.

4.4. Raman Spectra Analysis of 2ME

Figure 4d shows the most important vibrations of 2ME, corresponding to the range 1000–3200 cm^{-1}. In this range, the following features can be distinguished; the steroidal C-H and CH_2 groups located in the range from 2800 cm^{-1} to about 3100 cm^{-1}, and the OH band which absorbs in the zone of 1200–1350 cm^{-1}—this vibration mode is sensitive to hydrogen bonding. Alcohols and CH_3 groups are also located in this region. A broad peak could be observed around 1400–1500 cm^{-1} due to aromatic ring chain stretching vibrations of C-C-H and others at 1600 cm^{-1}, where the C=C aromatic ring chain vibrations are located [28,36,37]—both modes are possible to distinguish in IR spectra.

4.5. Raman Spectra Analysis of TiO_2–PEG–2ME

The Raman spectrum of the functionalized TiO_2 NPs which have been coated with PEG and loaded with 2ME is given in Figure 4e. This figure displays the Raman spectra above 1000 cm^{-1} (the low frequency bands of TiO_2 were not modified during the functionalization process). The Raman spectrum of TiO_2–PEG–2ME was slightly modified in the range of 1250–1450 cm^{-1} with respect to TiO_2–PEG (Figure 4c). In this range, we can find the resulting vibration mode between PEG and 2ME. The first band, located around 1300 cm^{-1}, corresponds to C-H vibration of PEG and O-H vibration of 2ME; this band became more broad in comparison with the band located in the same range in TiO_2–PEG (Figure 4c). The second band, located around 1447 cm^{-1}, corresponds to the vibration of C-H plus O-H vibration and the aromatic ring C-C-H vibration group of pure PEG and 2ME, respectively [28,37]. This band became more pronounced and defined due to the new hydrogen bridge bonding between PEG and 2ME. It was not possible to identify each the modes of vibration associated with the finger print of 2ME in TiO_2–PEG–2ME composite by the use of Raman spectroscopy. The bands corresponding to aromatic ring and functional groups located in the range 1500–1400 cm^{-1} and 1350–1200 cm^{-1}, respectively, were screened by the C-H vibration mode of PEG. Although a

change in form and intensity with respect to TiO_2–PEG is evident, this suggests the contribution of the functional groups of 2ME in the composite. However, the bands located around 1600 and 3000 cm^{-1} (corresponding to C=C aromatic ring chain vibrations and C-H groups) cannot be distinguished in the TiO_2–PEG–2ME nanocomposite. On the other hand, all these vibrations are clearly visible using FTIR spectroscopy.

5. 2ME Loading Capacity

Using the electrospray technique, we have determined that the percentage of loaded charge of 2ME into TiO_2–PEG is 9% with a stirring time of 180 min. It has been reported the encapsulation efficiency of 2ME in liposomes was around 8% [38], whereas other studies reported a 2ME encapsulation efficiency of around 3.3% in dendrimers [39]. 2-methoxyestradiol has been also encapsulated in PLGA (poly(DL-lactide-co-glycolic acid)) microparticles, giving a 11.6% 2ME-loading efficiency [40]; thus, our TiO_2–PEG–2ME carrier system showed similar loading efficiency as reported in other systems. On the other hand, nanoparticles combined with hydrophilic biodegradable polymers such PEG are non-immunogenic, non-antigenic, and protein resistant, shortening their bioavailability in the blood circulation, and therefore decreasing or eliminating the adsorption of the protein from the surface of the nanoparticle [41]. Furthermore, PEG is soluble in both polar and non-polar solvents, and it is highly soluble in cell membranes, suggesting that TiO_2–PEG–2ME nanoparticles have a high potential in biomedical applications.

6. Conclusions

This study shows for the first time the physicochemical characterization of conjugate TiO_2–PEG–2ME NPs. Using IR and Raman Spectra, it is possible to follow the modification processes attributed to the conjugation of PEG and 2ME to synthesized TiO_2 NPs step by step. 2ME has been considered a promising anticancer drug candidate due to its low toxicity and broad-spectrum anticancer activity; however, the clinical application of 2ME has been hampered by its low solubility, poor gastrointestinal absorption, shorter half-life, and low bioavailability [41]. Drug encapsulation showed that TiO_2–PEG–2ME can be a promising candidate for use in drug targeting delivery systems due to the reduced cytotoxicity of TiO_2 and the high solubility of PEG. In this context, our TiO_2–PEG–2ME composite can improve the disadvantages of 2ME, reinforcing its biomedical applications.

Acknowledgments: Proyecto Basal N° FB0807, Fondecyt Regular N° 1130950, Fondecyt N° 3140051. Proyecto PIIC, DGIP-UTFSM. ACT1108, Laboratorio de Síntesis de Nanomateriales: Dr. Patricio Habërle for providing access to the LabRAM spectrometer, Departamento de Física UTFSM. Center for Development of Nanoscience and Nanotechnology, CEDENNA.

Author Contributions: A.L. participated in the design of the study, carried out the characterization and funtionalization of the nanoparticles, analysis of data and writting the manuscript. P.R. participated in the synthesis of TiO_2 NP and functionalization of PEG-TiO_2 and TiO_2-PEG-2ME composites and performed the HPLC. C.G. performed the FTIR and RAMAN spectra and analysis of the data. R.S. participitaed in the realization of FTIR spectra and data analysis. P.V. analysis of the data and contribute to drafting the manuscript. P.Z. characterization of the TiO_2 NP, data analysis and drafting the manuscript. P.A.O. participated in the study design, analysis of the data and writing the manuscript.

Conflicts of Interest: The authors declare no conflict of interest.

References

1. Atefeh, G.T.; Nosrat, O. A comparative study on the nanoparticles for improved drug delivery systems. *J. Photochem. Photobiol. B Biol.* **2016**, *162*, 681–693.
2. Mahendra, R.; Avinash, P.; Inglea, I.; Adriano, B. Bioactivity of noble metal nanoparticles decorated with biopolymersand their application in drug delivery. *Int. J. Pharm.* **2015**, *496*, 159–172.
3. Dastjerdi, R.; Montazer, M. A review on the application of inorganic nano-structured materials in the modification of textiles: Focus on anti-microbial properties. *Colloids Surf. B* **2010**, *79*, 5–18.

4. Kubota, Y.; Shuin, T.; Kawasaki, C.; Hosaka, M.; Kitamura, H.; Cai, R.; Sakai, H.; Hashimoto, K.; Fujishima, A. Photokilling of T-24 human bladder cancer cells with Titanium dioxide. *Br. J. Cancer* **1994**, *70*, 1107–1111.
5. Sunkara, B.; Misra, R.D.K. Enhanced antibactericidal function of W^{4+} doped titania coated nickel ferrite composite nanoparticles A biomaterial system. *Acta Biomater.* **2008**, *4*, 273–283.
6. Venkatasubramanian, R.; Srivastava, R.; Misra, R.D.K. A comparative study of antimicrobial and photocatalytic activity of different dopants in titania encapsulated nanoparticle composites. *Mater. Sci. Technol.* **2008**, *24*, 589–595.
7. Rawat, J.; Rana, S.; Srivastava, R.; Misra, R.D.K. Antimicrobial activity of composite nanoparticles consisting of titania photocatalytic shell and nickel ferrite magnetic core. *Mater. Sci. Eng. C* **2007**, *27*, 540–545.
8. Kulkarni, M.; Mazare, M.; Gongadze, E.; Perutkova, S.; Kralj-Iglic, V.; Milosev, I.; Schmuki, P.; Iglic, A.; Mozetic, M. Titanium nanostructures for biomedical applications. *Nanotechnology* **2015**, *26*, 062002, doi:10.1088/0957-4484/26/6/062002.
9. Tianyi, W.; Haitao, J.; Long, W.; Qinfu, Z.; Tongying, J.; Bing, W.; Siling, W. Potential application of functional porous TiO_2 nanoparticles in light-controlled drug release and targeted drug delivery. *Acta Biomater.* **2015**, *13*, 354–363.
10. Jin, X.; Xiaobo, P.; Mengyan, W.; Jiong, M.; Yiyan, F.; Pei-Nan, W.; Lan, M. The role of surface modification for TiO_2 nanoparticles in cancer cells. *Colloids Surf. B Biointerfaces* **2016**, *143*, 148–155.
11. Yamaguchi, S.; Kobayashi, H.; Narita, T.; Kanehira, K.; Sonezaki, S.; Kudo, N.; Kubota, Y.; Terasaka, S.; Houkin, K. Sonodynamic therapy using water-dispersed TiO_2 polyethylene glycol compound on glioma cells: Comparison of cytotoxic mechanism with photodynamic therapy. *Ultrason. Sonochem.* **2011**, *18*, 1197–1204.
12. Qin, Y.; Sun, L.; Li, X.; Cao, Q.; Wang, H.; Tang, X.; Ye, L. Highly waterdispersible TiO_2 nanoparticles for doxorubicin delivery: Effect of loading mode on therapeutic efficacy. *J. Mater. Chem.* **2011**, *21*, 18003–18010.
13. Koch, S.; Kessler, M.; Mandel, K.; Dembski, K.; Heuze, S.; Hackenberg, S. Polycarboxylate ethers: The key towards non-toxic TiO_2 nanoparticles stabilisation in physiological solutions. *Colloids Surf. B Biointerfaces* **2016**, *143*, 7–14.
14. Naghibi, S.; Madaah, H.; Faghihi, M. Colloidal stability of dextran and dextran/poly ethylene glycol coated TiO_2 nanoparticles by hydrothermal assisted sol-gel method. *Ceram. Int.* **2013**, *39*, 8377–8384.
15. Mano, S.; Kanehira, K.; Sonezaki, S.; Taniguchi, A. Effect of polyethylene glycol modication of TiO_2 nanoparticles on cytotoxicity and gene expressions in human cell lines. *Int. J. Mol. Sci.* **2012**, *13*, 3703–3717.
16. Devanand, G.; Ramasamy, S.; Ramakrishnan, B.; Kumar, J. Folate targeted PEGylated titanium dioxide nanoparticles as a nanocarrier for targeted paclitaxel drug delivery. *Adv. Powder Technol.* **2013**, *24*, 947–954.
17. Sanaz, N.; Hamid, R.; Mohammad, F.; Mhammad, S.; Morteza, M. Mortality response of folate receptor-activated, PEG-functionalized TiO_2 nanoparticles for doxorubicin loading with and without ultraviolet irradiation. *Ceram. Int.* **2014**, *40*, 5481–5488.
18. Parada-Bustamante, A.; Valencia, C.; Reuquen, P.; Diaz, P.; Rincon-Rodriguez, R.; Orihuela, P.A. Role of 2-methoxyestradiol, an endogenous estrogen metabolite, in health and disease. *Mini Rev. Med. Chem.* **2015**, *15*, 427–438.
19. Guohua, X.; Baoan, C.; Jiahua, D.; Chong, G.; Huixia, L.; Zeye, S.; Feng, G.; Xuemei, W. Effect of magnetic Fe_3O_4 nanoparticles with 2-metoxyestradiol, on the cell-cycle progression and apoptosis of myelodysplastic syndrome cells. *Int. J. Nanomed.* **2011**, *6*, 1921–1927.
20. Shi, J.; Wang, Z.; Wang, L.; Wang, H.; Li, L.; Yu, X.; Zhang, J.; Ma, R.; Zhang, Z. Photodynamic therapy of a 2-methoxyestradiol tumor-targeting drug delivery system mediated by Asn-Gly-Arg in breast cancer. *Int. J. Nanomed.* **2013**, *8*, 1551–1562.
21. Wang, Y.; Guo, R.; Cao, X.; Shen, M.; Shi, X. Encapsulation of 2-methoxyestradiol within multifunctional poly(amidoamine) dendrimers for targeted cancer therapy. *Biomaterials* **2011**, *32*, 3322–3329.
22. Jang, L.; Liu, Y.; Zeng, G.; Xiao, F.; Hu, X.-J.; Hu, X.; Wang, H.; Li, T.; Zhou, L.; Tan, X. Removal of 17b-estradiol by few-layered graphene oxide nanosheets from aqueous solutions: External influence and adsorption mechanism. *Chem. Eng. J.* **2016**, *284*, 93–102.
23. Mahshid, S.; Askari, M.; Ghamsari, M. Synthesis of TiO_2 nanoparticles by hydrolysis and peptization of titanium isopropoxide solution. *J. Mater. Process. Technol.* **2007**, *189*, 296–300.
24. Zapata, P.; Palza, H.; Rabagliati, F.M. Novel antimicrobial polyethylene composites prepared by metallocenic in situ polymerization with TiO_2 based nanoparticles. *J. Polym. Sci.* **2012**, *50*, 4055–4062.

25. Putz, H.; Brandenburg, K. Diamond-crystal and molecular structure visualization. *Cryst. Impact-GbR* **2006**, *102*, 53227.
26. Nadica, D.; Abazovic, M.; Comor, M.; Dramicanin, D.;. Jovanovic, S.; Jovan, M. Photoluminescence of Anatase and Rutile TiO_2 Particles. *J. Phys. Chem. B* **2006**, *110*, 25366–25370.
27. Mugundan, S.; Rajamannan, G.; Viruthagiri, N.; Shanmugam, R.; Gobi, P. Synthesis and characterization of undoped and cobalt-doped TiO_2 nanoparticles via sol-gel technique. *Appl. Nanosci.* **2015**, *5*, 449–456.
28. Colthup, N.; Daly, L.; Wiberley, S. *Introduction to Infrared and Raman Spectroscopy*; Academic Press: Boston, MA, USA, 1990.
29. Choi, H.C.; Young, M.; Seung, B. Size effects in the Raman spectra of TiO_2 nanoparticles. *Vib. Spect.* **2005**, *37*, 33–38.
30. Ohsaka, T. Temperatura dependence of the Raman spectrum in anatase TiO_2. *J. Phys. Soc. Jpn.* **1980**, *48*, 1661.
31. Zhu, K.R.; Zhang, M.S.; Chen, Q.; Yin, Z. Size and phonon-confinement effects on low-frequency Raman mode of anatase TiO_2 nanocrystal. *Phys. Lett. A* **2005**, *340*, 220–227.
32. Jin, Y.; Sun, M.; Mu, D.; Ren, X.; Wang, Q.; Wen, L. Investigation of PEG adsorption on copper in Cu_2+ free solution by SERS and AFM. *Electrochim. Acta* **2012**, *78*, 459–465.
33. Constantinescu, M.; Dumitrache, D.; Constantinescu, E.; Anghel, V.; Popa, M. Latent heat nano composite building materials. *Eur. Polym. J.* **2010**, *46*, 2247–2254.
34. Marek, K. Conformational changes in the chains of polyoxyethylene glycols. *J. Mol. Liq.* **2006**, *128*, 105–107.
35. Yamini, D.; Devanand, G.; Kumar, J.; Ramakrishnan, V. Raman scattering studies on PEG functionalized hydroxyapatite nanoparticles. *Spectrochim. Acta Part A Mol. Biomol. Spectrosc.* **2014** , *117*, 299–303.
36. Rui ,W.; Hyangah, C.; Sangyeop, L.; Ziyi, C.; Sung, H.; Young, H.; Jaebum, C. Highly sensitive detection of hormone estradiol E2 using surface enhanced Raman scattering based immunoassays for the clinical diagnosis of precocious puberty. *Appl. Mater. Interfaces* **2016**, *8*, 10665–10672.
37. Variankaval, N.; Jacob, K.; Dinh, S. Characterization of crystal forms of 2-mestradiol thermal analysis, Raman microscopy, X-ray analysis and solid-state NMR. *J. Cryst. Growth* **2000**, *217*, 320–331.
38. Du, B.; Li, Y.; Youmei, A.; Chen, Ch.; Zhang, Z. Preparation, characterization and in vivo evaluation of 2-methoxyestradiol-loaded liposomes. *Int. J. Pharmacol.* **2010**, *384*, 140–147.
39. Du, B.; Wang, S.; Shi, S.; Zhang, C.; Zhang, Z. The effect of 2-methoxyestradiol liposome on growth inhibition, angiogenesis and expression of VEGF and Ki67 in mice bearing H22 hepatocellular carcinoma. *Tumori* **2011**, *97*, 660–665.
40. Guo, X.; Mei, Q.; Xing, Y.; Ye, L.; Zhang, H.; Shi, X.; Zhang, Z. Preparation and cytotoxicity of poly (DL-lactide-co-glycolide) microspheres encapsulating 2-methoxyestradiol. *Drug Deliv.* **2011**, *19*,143–148.
41. Guo, X.; Zhang, N.; Cui, F.; Du, B.; Zhang, Z. An investigation on intestinal absorption of a new anticancer drug, 2-methoxyestradiol. *Pharmazie* **2009**, *64*, 748–751.